Analytical Chemistry
August 15, 2009
Volume 81, Issue 16
Pages 6563-7126

About the Cover:

The cover shows a molecular dynamics simulation of the interaction of a 5 keV organic nanodrop (~5 nm diameter) with a polymeric surface (top) before impact and (bottom) 20 ps after impact. Such projectiles with less than 1 eV of energy per nucleon can desorb intact kilodalton molecules with minimal fragmentation. The article is by Arnaud Delcorte, Barbara Garrison, and Karim Hamraoui. (Art by Arnaud Delcorte)

Anal. Chem. **2009,** *81,* 6676–6686

Dynamics of Molecular Impacts on Soft Materials: From Fullerenes to Organic Nanodrops

A. Delcorte,*,† B. J. Garrison,‡ and K. Hamraoui†

Unité PCPM, Université Catholique de Louvain, 1 Croix du Sud, B-1348, Louvain-la-Neuve, Belgium, and Department of Chemistry, The Pennsylvania State University, University Park, Pennsylvania 16802

The present theoretical study explores the interaction of various energetic molecular projectiles and clusters with a model polymeric surface, with direct implications for surface analysis by mass spectrometry. The projectile sizes (up to 23 kDa) are intermediate between the polyatomic ions (SF_5, C_{60}) used in secondary ion mass spectrometry and the large organic microdroplets generated, for example, in desorption electrospray ionization. The target is a model of amorphous polyethylene, already used in a previous study [Delcorte, A.; Garrison, B. J. *J. Phys. Chem. C* 2007, *111*, 15312]. The chosen method relies on classical molecular dynamics (MD) simulations, using a coarse-grained description of polymeric samples for high energy or long time calculations (20−50 ps) and a full atomistic description for low energy or short time calculations (<1 ps). Two regions of sputtering or desorption are observed depending on the projectile energy per nucleon (i.e., effectively the velocity). The transition, occurring around 1 eV/nucleon, is identified by a change of slope in the curve of the sputtering yield per nucleon vs energy per nucleon. Beyond 1 eV/nucleon, the sputtering yield depends only on the total projectile energy and not on the projectile nuclearity. Below 1 eV/nucleon, i.e., around the sputtering threshold for small projectiles, yields are influenced by both the projectile energy and nuclearity. Deposition of intact molecular clusters is also observed at the lowest energies per nucleon. The transition in the sputtering curve is connected to a change of energy deposition mechanisms, from atomistic and mesoscopic processes to hydrodynamic flow. It also corresponds to a change in terms of fragmentation. Below 1 eV/nucleon, the projectiles are not able to induce bond scissions in the sample. This region of molecular emission with minimal fragmentation offers new analytical perspectives, out of reach of smaller molecular clusters such as fullerenes.

As shown by the recent literature, there is a plethora of possible projectiles for surface mass spectrometry,[1,2] including, for instance, small metal clusters,[3,4] light-element clusters,[5−7] ionic materials[8] or large noble gas clusters,[9] and metal nanoparticles.[10,11] Polyatomic ions such as SF_5^+ and C_{60}^+ have already proved to be very useful for molecular depth profiling and, ultimately, 3D molecular imaging of solid organic samples.[5,6] In competition with light-element molecular ions, primary ion beams of metal clusters such as Au_n^+ and Bi_n^+, which can be better focused (<50 nm), also constitute excellent candidates for high-resolution molecular imaging.[3,4] Most probably, the various applications of secondary ion mass spectrometry (SIMS) in biology, materials science, or nanotechnology will require different projectiles and/or a combination of projectiles, e.g., a light-element molecular beam for profiling with limited damage and a better focused liquid-metal cluster ion beam for analysis.[12,13]

The experimental investigation of new ion beams and guns, however, is costly and time-consuming. As long as the dynamics of molecular emission remains central, rather than electronic effects, computer simulation methods constitute an adequate substitute to predict the major observations. In addition, they are the only way to explore the underlying microscopic mechanisms.[14] Among the many theoretical studies,[15−21] only a few address the issue of bulk organic materials, which represent a large area of application in SIMS. In general, the focus has been placed mostly

* To whom correspondence should be addressed. E-mail: arnaud.delcorte@uclouvain.be.
† Université Catholique de Louvain.
‡ The Pennsylvania State University.

(1) McDonnell, L. A.; Heeren, R. M. A. *Mass Spectrom. Rev.* **2007**, *26*, 606.
(2) De Mondt, R.; Van Vaeck, L.; Heile, A.; Arlinghaus, H. F.; Nieuwjaer, N.; Delcorte, A.; Bertrand, P.; Lenaerts, J.; Vangaever, F. *Rapid Commun. Mass Spectrom.* **2008**, *22*, 1481.
(3) Kollmer, F. *Appl. Surf. Sci.* **2004**, *231−232*, 153.
(4) Delcorte, A. *Appl. Surf. Sci.* **2008**, *255*, 954.
(5) Gillen, G.; Fahey, A.; Wagner, M.; Mahoney, Ch. *Appl. Surf. Sci.* **2006**, *252*, 6537.
(6) Fletcher, J. S.; Rabbani, S.; Henderson, A.; Blenkinsopp, P.; Thompson, S. P.; Lockyer, N. P.; Vickerman, J. C. *Anal. Chem.* **2008**, *80*, 9058.
(7) Winograd, N. *Anal. Chem.* **2005**, *77*, 142A.
(8) Dienhelt, C. W.; Van Stipdonk, M. J.; Schweikert, E. A. *Nucl. Instrum. Methods Phys. Res., Sect. B* **1998**, *142*, 606.
(9) Matsuo, J.; Okubo, Ch.; Seki, T.; Aoki, T.; Toyoda, N.; Yamada, I. *Nucl. Instrum. Methods Phys. Res., Sect. B* **2004**, *219*, 463.
(10) Li, Zh.; Verkhoturov, S. V.; Locklear, J. E.; Schweikert, E. A. *Int. J. Mass Spectrom.* **2008**, *269*, 112.
(11) Rajagopalachary, S.; Verkhoturov, S. V.; Schweikert, E. A. *Nano Lett.* **2008**, *8*, 1076.
(12) Breitenstein, D.; Rommel, Ch. E.; Mollers, R.; Wegener, J.; Hagenhoff, B. *Angew. Chem., Int. Ed.* **2007**, *46*, 5332–5335.
(13) Wucher, A. *Appl. Surf. Sci.* **2006**, *252*, 6482.
(14) Garrison, B. J. In *ToF-SIMS: Surface Analysis by Mass Spectrometry*; Vickerman, J. C., Briggs, D., Eds.; SurfaceSpectra/IMPublications: Chichester, U.K., 2001; p 223.
(15) Garrison, B. J.; Postawa, Z. *Mass Spectrom. Rev.* **2008**, *27*, 289.
(16) Aoki, T.; Seki, T.; Ninomiya, S.; Matsuo, J. *Appl. Surf. Sci.* **2008**, *255*, 944.
(17) Webb, R. P.; Ponomarev, M. *Nucl. Instrum. Methods Phys. Res., Sect. B* **2008**, *255*, 229.

10.1021/ac900746x CCC: $40.75
Published on Web 07/06/2009

on relatively small clusters, with a mass typically below 1 kDa, or on massive gas or metal clusters (nanoparticles). The choice of projectiles, e.g., C_{60},[15,21,22] Au_n,[22,23] Ar_n,[24−26] was often dictated by the concomitant experimental application in SIMS and related techniques.

Rather than the collision cascade theory, valid for atomic projectiles, the processes induced under cluster impact are often rationalized using fluid dynamics arguments.[22] Unlike atomic projectiles, small clusters with energies of 5−100 keV always create craters at the sample surface. Beyond a certain threshold, the crater size and the induced sputtering yield were predicted to increase linearly with the total kinetic energy.[19,21,23,27] Massive clusters in the same energy range create craters or not, depending on the target material and on the energy per constituent in the projectile.[24,28,29] For strongly bound (covalent, metallic) clusters, this change of behavior corresponds approximately to the frontier with soft-landing, i.e., when the acceleration energy per atom becomes lower than the binding energy of the cluster constituents.[30] At higher energy, cluster implantation occurs when the projectile constituents bury significantly deeper than the forming crater.[28] In the case of gold clusters impinging on gold, the transition between microscopic and macroscopic cratering (meteorite impacts) was recently predicted to arise for clusters in the range $Au_{1\,000}$−$Au_{10\,000}$ with typical meteoroid velocities (∼20 km/s).[31]

A series of theoretical studies have been devoted to the comparison of light-element clusters, essentially fullerenes, impinging on a bulk organic sample, benzene.[19,20,32,33] At 5 keV, a maximum of molecular emission is observed between C_{20} and C_{60} and the yields decrease slightly for larger clusters up to C_{180} (2.2 kDa).[19] For higher kinetic energies, the maximum shifts to larger cluster sizes.[20] The results are explained by the size of the ejection cone derived from the distribution of the projectile energy in the surface shortly after impact (mesoscopic energy deposition footprint or MEDF model[22,34]). In all cases, small clusters such as C_6H_6 and $C_{10}H_8$ provide slightly lower yields of benzene molecules. For fullerenes, the slowing of the projectile in benzene is comparable to the effect of friction on a single particle with the mass and size of the cluster.[33]

The explanation of the performance of fullerenes lies in their small atomic mass and relatively large nuclearity, which allows them to deposit all their energy in the surface region of organic samples, maximizing the molecular yield via collective emission processes and minimizing damage in the depth of the sample.[20,35] At the other end of the spectrum in terms of size, the nano- and microdroplets used in massive cluster impact (MCI),[36] electrospray desorption ionization (EDI),[37,38] impact desolvation of electrosprayed microdroplets (IDEM),[39] and desorption electrospray ionization (DESI)[40,41] have also proved to be outstanding for intact organic molecule emission. Therefore, the question arises whether carbon-based clusters with an intermediate size could also be of interest for organic mass spectrometry. From a fundamental viewpoint, this investigation should help bridge the gap between the domains of small keV cluster bombardment and large molecular cluster impacts. These considerations constitute the motivation of the present study. The chosen series of six projectiles includes coronene (0.3 kDa), kilodalton hydrocarbons and a molecular cluster (23 kDa) where "test" kilodalton molecules are embedded in a low-molecular weight matrix. Even though our range of investigations is restricted to relatively small nanoclusters (<5 nm diameter), in order to limit computational expenses, the energy per nucleon in our largest projectiles is comparable to those used in EDI and MCI (<1 eV/nucleon). Using the same amorphous polyethylene oligomer sample as in a previous study[21] allows us to generalize some of the results obtained upon C_{60} bombardment of polymers.

This article explores the different situations of sputtering, fragmentation, and molecular deposition induced by such hydrocarbon projectiles, with ∼0.3−15 keV of kinetic energy. We identify a transition in the yield vs energy per nucleon curve at 1 eV/nucleon and explain its connection with the unique region below 1 eV/nucleon, in which there is intact molecular ejection without concurrent sputtered fragments. The calculated indicators of emission and fragmentation are rationalized on the basis of the dynamics of energy deposition in the surface region. A special emphasis is placed on free hydrogen creation in the surface, originating either from the projectile or the sample. Indeed, H atoms generally play a special role in the ionization process of desorbed molecules in surface-based mass spectrometry methods.[13] In addition to mass spectrometry, our results have implications in the field of cluster beam-induced modification of organic materials and, in particular, for the methods of soft-landing and reactive-landing.[42−45]

(18) Baranova, I.; Della-Negra, S.; Domaratsky, V.; Chemezov, A.; Novikov, A.; Obnorsky, V.; Pautrat, M.; Anders, Ch.; Urbassek, H. M.; Wien, K.; Yarmiychuk, S.; Zhurkin, E. *Nucl. Instrum. Methods Phys. Res., Sect. B* **2008**, *266*, 1993.
(19) Smiley, E.; Winograd, N.; Garrison, B. J. *Anal. Chem.* **2007**, *79*, 494.
(20) Ryan, K. E.; Garrison, B. J. *Anal. Chem.* **2008**, *80*, 6666.
(21) Delcorte, A.; Garrison, B. J. *J. Phys. Chem. C* **2007**, *111*, 15312.
(22) Russo, M. J., Jr.; Garrison, B. J. *Anal. Chem.* **2006**, *78*, 7206.
(23) Anders, Ch.; Urbassek, H. M.; Johnson, R. E. *Phys. Rev. B* **2004**, *70*, 155404.
(24) Rzeznik, L.; Czerwinski, B.; Garrison, B. J.; Winograd, N.; Postawa, Z. *J. Phys. Chem. C* **2008**, *112*, 521.
(25) Samela, J.; Nordlund, K. *New J. Phys.* **2008**, *10*, 023013.
(26) Aoki, T.; Seki, T.; Ninomiya, S.; Matsuo, J. *Surf. Coat. Technol.* **2007**, *201*, 8427.
(27) Zimmermann, S.; Urbassek, H. M. *Nucl. Instrum. Methods Phys. Res., Sect. B* **2007**, *255*, 208.
(28) Nordlund, K.; Jarvi, T. T.; Meinander, K.; Samela, J. *Appl. Phys. A: Mater. Sci. Process.* **2008**, *91*, 561.
(29) Aoki, T.; Matsuo, J. *Nucl. Instrum. Methods Phys. Res., Sect. B* **2006**, *242*, 517.
(30) Popok, V. N.; Campbell, E. E. B. *Rev. Adv. Mater. Sci.* **2006**, *11*, 19.
(31) Samela, J.; Nordlund, K. *Phys. Rev. Lett.* **2008**, *101*, 027601.
(32) Smiley, E.; Postawa, Z.; Wojciechowski, I. A.; Winograd, N.; Garrison, B. J. *Appl. Surf. Sci.* **2006**, *252*, 6436.
(33) Garrison, B. J.; Ryan, K. E.; Russo, M. F., Jr.; Smiley, E. J.; Postawa, Z. *J. Phys. Chem. C* **2007**, *111*, 10135.
(34) Russo, M. J., Jr.; Szakal, C.; Kozole, J.; Winograd, N.; Garrison, B. J. *Anal. Chem.* **2007**, *79*, 4493.
(35) Delcorte, A.; Garrison, B. J. *Nucl. Instrum. Methods Phys. Res., Sect. B* **2007**, *255*, 223.
(36) Cornett, D. S.; Lee, T. D.; Mahoney, J. F. *Rapid Commun. Mass Spectrom.* **1994**, *8*, 996.
(37) Hiraoka, K.; Mori, K.; Asakawa, D. *J. Mass Spectrom.* **2006**, *41*, 894.
(38) Asakawa, D.; Fujimaki, S.; Hashimoto, Y.; Mori, K.; Hiraoka, K. *Rapid Commun. Mass Spectrom.* **2007**, *21*, 1579.
(39) Aksyonov, S. A.; Williams, P. *Rapid Commun. Mass Spectrom.* **2001**, *15*, 2001.
(40) Takats, Z.; Wiseman, J. M.; Cooks, R. G. *J. Mass Spectrom.* **2005**, *40*, 1261.
(41) Kauppila, T. J.; Wiseman, J. M.; Ketola, R. A.; Kotiaho, T.; Cooks, R. G.; Kostiainen, R. *Rapid Commun. Mass Spectrom.* **2006**, *20*, 387.
(42) Wang, P.; Hadjar, O.; Gassmana, P. L.; Laskin, J. *Phys. Chem. Chem. Phys.* **2008**, *10*, 1512.

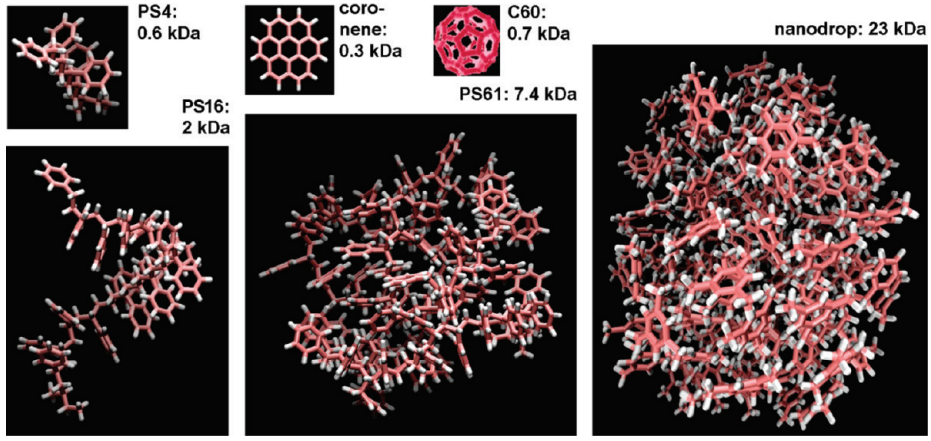

Figure 1. Set of molecular projectiles used in the simulations. See Table 1 for more details.

COMPUTATIONAL METHOD

In order to describe the time-evolution of the system at the microscopic level, Hamilton's equations of motion are numerically integrated over some time interval, providing us with the position and velocity of each particle at each time step.[14] Forces among the atoms or particles in the system are derived from semiempirical interaction potentials whose careful choice constitutes the key of a realistic description of the studied mechanisms. In order to reduce the computational expense, in most of the simulations presented here, certain atoms of the sample are grouped to form united atoms or particles. One advantage of such a coarse-grained approach is that the calculation time is significantly reduced because of the smaller number of particles and the simpler potentials. Furthermore, the fast H-vibration is eliminated, which allows for a larger time step to be used in the integration.[32,46] With this prescription, the large systems required to realistically describe the interactions of large energetic clusters with organic solids can be treated within reasonable computation times. Validation of the model by comparison with an atomistic model using the many-body AIREBO potential[47] was successfully achieved in the case of C_{60} bombardment of benzene molecular solids.[32] To address specific issues, such as the quantity of free hydrogen atoms generated in the solid, short-term fully atomistic simulations were also performed using a limited size system.

The specifics of the computational cell used for the coarse-grained simulations of an amorphous polyethylene (PE) oligomer molecular sample have been described in detail in ref 21. Briefly, the sample was a box containing $\sim 4 \times 10^5$ united atoms, forming $\sim 4 \times 10^3$ molecules, where each molecule was a string of 97 CH_2 particles of 14 amu and capped with 2 CH_3 particles of 15 amu. With the chosen potentials, the final density of the relaxed PE solid was 1.01 g/cm^3. In all the sputtering calculations, a stochastic region at 0 K and a rigid layer were put on five sides of the sample in order to absorb the pressure waves induced by the projectiles.[48] Most of the simulations involving the coarse-grained PE were stopped at 20 ps except for a few check cases where the trajectory time was extended up to 50 ps.

A series of trajectories were also calculated using an atomistic description of the sample. The goal of these simulations was to investigate the projectile energy transfer to the target and, in particular, the scission of bonds and creation of free H atoms in the sample. These simulations were restricted to the first picosecond of the interaction and, therefore, a much smaller sample could be used. The sample was a quasi-cubic box containing 24 800 atoms in 400 polyethylene molecules each composed of 20 C atoms and 42 H atoms (icosane). The density of this sample was 0.90 g/cm^3. The reason why shorter chains were preferred is purely practical, that is, such short chains allowed us to obtain a relaxed sample of the desired size with a reasonably regular shape (cube). Even though icosane molecules are 5 times shorter than the PE molecules used in the coarse-grained system, the structure is slightly different and the atomic fraction of hydrogen is slightly higher (67.7% for icosane against 66.9% for the longer polyethylene sample), we feel that the difference is sufficiently small to be neglected, at least in first approximation, with respect to the goal of this part of the study. Open boundary conditions were used in these simulations.

The molecular projectiles used in this study are shown in Figure 1, and their main characteristics are listed in Table 1. They were described at the atomistic scale for all the performed simulations, whether the sample was coarse-grained or not. They consist of a single molecule except for the nanodrop, which contains four polystyrene molecules in a low-molecular weight matrix (trimethylbenzene).[49] For both the projectiles and the atomistic sample, hydrogen ^{1}H is replaced by tritium ^{3}H for computational efficiency. The masses and number of nucleons of the different projectiles in Table 1 were calculated accordingly. In all the simulations, the incidence angle of the projectiles is normal.

In the coarse-grained model, a Lennard−Jones potential was used to describe the interactions of the particles located on different molecules. The values of ε and σ were chosen from

(43) Ouyang, Zh.; Takáts, Z.; Blake, Th. A.; Cologan, B.; Guymon, A. J.; Wiseman, J. M.; Oliver, J. C.; Davisson, V. J.; Cooks, R. G. *Science* **2003**, *301*, 1351.
(44) Goto, M.; Zhigilei, L.; Hobley, J.; Kishimoto, M.; Garrison, B. J.; Fukumura, H. *J. Appl. Phys.* **2001**, *90*, 4755.
(45) Serra, P.; Fernandez-Pradas, J. M.; Berthet, F. X.; Colina, M.; Elvira, J.; Morenza, J. L. *Appl. Phys. A: Mater. Sci. Process.* **2004**, *79*, 949.
(46) Delcorte, A.; Garrison, B. J. *Nucl. Instrum. Methods Phys. Res., Sect. B* **2007**, *255*, 223.
(47) Stuart, S. J.; Tutein, A. B.; Harrison, J. A. *J. Chem. Phys.* **2000**, *112*, 6472.
(48) Garrison, B. J.; Kodali, P. B. S.; Srivastava, D. *Chem. Rev.* **1996**, *96*, 1327.
(49) Delcorte, A.; Garrison, B. J. *J. Phys. Chem. B* **2003**, *107*, 2297.

Table 1. Properties of the Selected Molecular Projectiles

	coronene	PS4	C_{60}	PS16	PS61	nanodrop
mass[a] (Da) [nucleons]	324.4 [324]	558.7 [558]	720.7 [720]	2000.6 [1998]	7407.4 [7398]	22 998.5 [22 968]
no. of C atoms	24	36	60	132	492	1464
no. of H atoms	12	42	0	138	498	1800
no. of molecules	1	1	1	1	1	108[d]
projectile size (nm)						
X	0.9[b]−0.9[c]	1.7	0.7	2.2	3.1	4.0
Y	0.1[b]−0.9[c]	0.9	0.7	1.9	3.1	3.9
Z	0.9[b]−0.1[c]	0.9	0.7	2.7	3.0	4.4
potential energy (keV)	−0.2	−0.4	−0.4	−1.3	−4.9	−15.6
energy/nucleon at 10 keV (eV)	30.9	17.9	13.9	5.0	1.4	0.4
velocity at 10 keV (km/s)	77	59	52	31	16	9

[a] Tritium (three nucleons) is used instead of hydrogen for computer efficiency. [b] Vertical orientation. [c] Horizontal orientation. [d] 4 PS16 molecules and 104 trimethylbenzene (C_9H_{12}) molecules.

previous studies describing linear hydrocarbons.[50,51] The intermolecular binding energy of a bulk PE molecule was ~9 eV. For the intramolecular interactions, the model must allow molecules to store internal energy up to the point when they dissociate. As was previously described, a Morse potential[52] between adjacent CH_2 and CH_3 particles was chosen to account for the dissociating bond stretch term, with parameters that reflect the bond strength and equilibrium distance in linear hydrocarbons.[50,51] The other interactions were between CH_x particles separated by one CH_x particle, which were modeled by a Morse potential with a small well depth.[46] This pair potential allows the particles to interact if the molecule is dissociated and also provides an equilibrium configuration of the sample in which the molecules adopt the appropriate zigzag shape. This type of interaction was preferred to an angle bend term that does not allow for dissociation and would therefore be limiting for sputtering simulations. For CH_x particles of a molecule that were separated by two or more particles, a Lennard−Jones potential with the same parameters as the one used for intermolecular interactions was used. The Morse and Lennard−Jones potential parameters can be found in ref 21. A weak Lennard−Jones potential was used between the C,H atoms of the projectiles and the CH_x particles of the molecular sample. In all the simulations, the AIREBO potential was used to describe the C−C and the C−H interactions within the fullerene and the hydrocarbon projectiles.[47,53] In the fully atomistic simulations, that same potential was used to describe the interactions between all the atoms, including those atoms within the target.

RESULTS AND DISCUSSION

In this article, the effects of molecular projectile impacts on polyethylene surfaces are considered from different viewpoints. First, yields of molecules and fragments are discussed as a function of the projectile type and kinetic energy. This analysis leads to the identification of two domains with different physical and chemical processes which are discussed next. Finally, we consider free hydrogen atom formation in the energized nanovolume of the target surface.

Sputtering Yields and Sputtering Regions. Various combinations of yields vs energy or energy per nucleon are given in Figures 2 and 3. In all cases, the symbol shape represents the incident kinetic energy and the symbol color the projectile type. Figure 2 displays the net sputtered mass, the number of intact molecules (i.e., not fragmented) and the number of fragments ejected as a function of incident kinetic energy. The net sputtered mass given in Figure 2a corresponds to the difference in the mass of the sputtered target plus the mass of the backscattered portions of the projectile minus the mass of the deposited portions.

In general, the yields are linear with increasing energy for the larger energies. The net yields for the smaller clusters are virtually identical, but for PS61 the yields are lower and for the nanodrop there is net deposition of material. The changes with mass will be discussed further below. The yield of intact ejected molecules (Figure 2b) and fragments (Figure 2c) follow similar linear trends. All the clusters except the nanodrop eject similar numbers of intact molecules. For the fragments, however, the three larger projectiles give reduced numbers of fragments relative to the smaller projectiles.

A transition between regions of net deposition and net erosion of the target was also experimentally observed[54] for C_{60} clusters impinging on silicon. In simulations of kiloelectronvolt C_{60} bombardment of silicon and carbon containing materials,[55−57] the projectile dissociates upon impact and strong covalent bonds are formed between atoms in the projectile and atoms in the substrate. At lower incident kinetic energies, the number of sputtered substrate atoms is smaller than the number of projectile atoms implanted in the substrate and, therefore, there is a net deposition of material. In the case presented in this study, the slow moving projectiles remain intact during the initial impact with the surface. The projectile loses its kinetic energy to the substrate atoms and is left with an insufficient amount of energy to eject.

The data in Figure 2 have been plotted in a form that is comfortable comparing to experimental conditions. As shown previously,[20,23] common features of the yields are more illustrative if the yield is plotted vs scaled coordinates, Figure 3. These previous studies used reduced units of energy (and yield) per

(50) Hautman, J.; Klein, M. L. *J. Chem. Phys.* **1989**, *91*, 4994.
(51) Balasubramanian, S.; Klein, M. L.; Siepmann, J. I. *J. Chem. Phys.* **1995**, *103*, 3184.
(52) Girifalco, L. A.; Weizer, V. G. *Phys. Rev.* **1959**, *114*, 687.
(53) Brenner, D. W.; Shenderova, O. A.; Harrison, J. A.; Stuart, S. J.; Ni, B.; Sinnott, S. B. *J. Phys.: Condens. Matter* **2002**, *14*, 783.
(54) Gillen, G.; Batteas, J.; Michaels, C. A.; Chi, P.; Small, J.; Windsor, E.; Fahey, A.; Verkouteren, J.; Kim, K. J. *Appl. Surf. Sci.* **2006**, *252*, 6521.
(55) Krantzman, K. D.; Kingsbury, D. B.; Garrison, B. J. *Appl. Surf. Sci.* **2006**, *252*, 6463.
(56) Krantzman, K. D.; Kingsbury, D. B.; Garrison, B. J. *Nucl. Instrum. Methods Phys. Res., Sect. B* **2007**, *255*, 238.
(57) Krantzman, K. D.; Garrison, B. J. *J. Phys. Chem. C* **2008**, *113*, 3239.

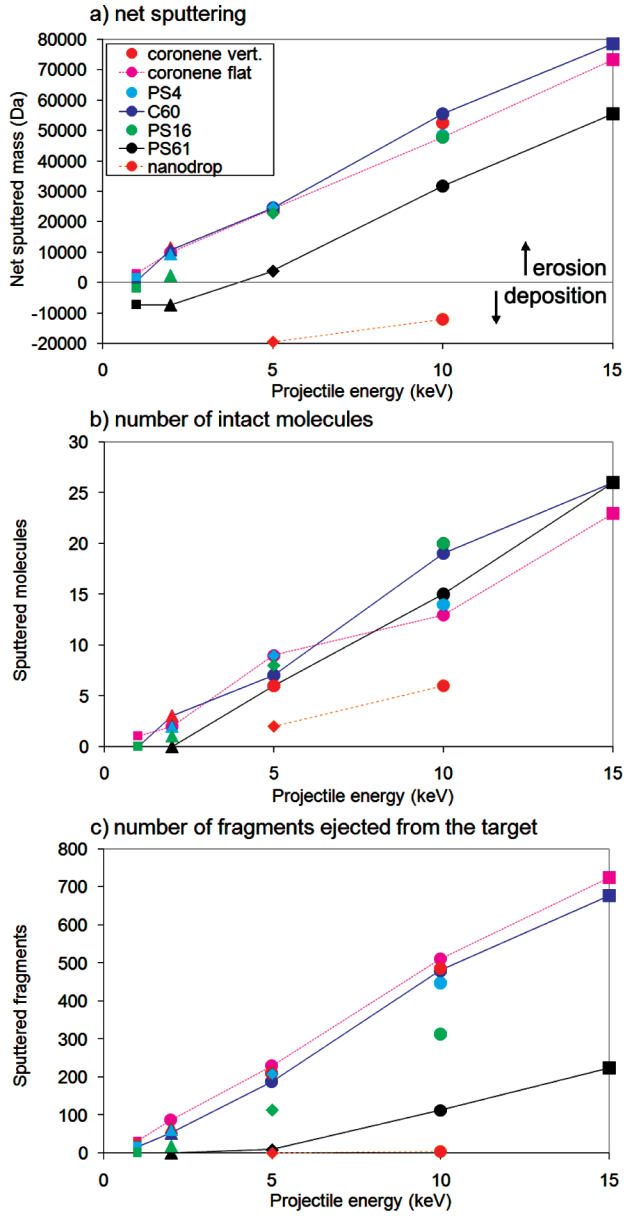

Figure 2. Energy-dependence of the sputtering for molecular projectiles. (a) Net sputtered mass (sputtered plus backscattered minus deposited); (b) number of intact molecules ejected; (c) number of fragments sputtered from the target. Color coding determines the projectile (see legend in Figure 2a). Symbol shapes refer to the total energy of the projectiles: 1 keV, small squares; 2 keV, triangles; 5 keV, diamonds; 10 keV, circles; and 15 keV, large squares.

number of particles in the projectile. In this case, there are two kinds of atoms with different masses in the projectile, thus units of energy per nucleon are used. The physics behind using the energy per nucleon is that the quantity is related to the velocity of the projectile as shown in the upper scale in Figure 3a,c.

The ejected mass per nucleon and the total ejected mass are shown in Figure 3a,b. Figure 3a is only for the mass sputtered from the target and does not include deposited material as in Figure 2a. The ejected mass per nucleon vs energy per nucleon (Figure 3a) exhibits a linear region (high energy part). The change of slope in the curve indicates a transition between two regions of sputtering, approximately below and above 1 eV/nucleon. It is important to recognize that, even though there appears to be one continuous curve in Figure 3a, each projectile contributes to different portions of the curve. For the small projectiles (coronene, PS4, C_{60}, PS16), the experimentally accessible energy range of 1−15 keV translates to electronvolt/nucleon values of >∼1 eV/nucleon. In fact, at energies equivalent to <1 eV/nucleon, most of these smaller projectiles sputter little or no target material, as indicated by the arrows at the bottom of Figure 3a. In order to obtain small energies per nucleon while maintaining the total kinetic energy in the 5−10 keV range, the mass of the projectile must be in the range of tens of kilodaltons as with the nanodrop. This particle, however, does not give rise to any of the data points in the greater than 1 eV/nucleon region. The data for PS61 span the transition region, connecting with the nanodrop data on the low-energy side and to the smaller cluster data on the high-energy side. The linear region of Figure 3a translates into a plateau in Figure 3b, in terms of total sputtered mass for a given projectile energy, i.e., the sputtered mass depends only on the total energy of the projectile and not on its nuclearity.

The observation that there is a threshold like behavior in the yield per nucleon vs energy per nucleon has been identified previously for simulations of atomic cluster projectiles bombarding atomic solids.[23] The domain before the threshold was described as the onset region, spreading over different energy ranges for different projectile sizes. In our simulations, the transition corresponds to a change in the rate at which the energy is deposited into the substrate, as will be shown in Microscopic View. For the region above 1 eV/nucleon, previous simulations have shown that the energy of the projectile is deposited in a 2−4 nm depth in a time < ∼100 fs.[20,22,58] As an approximate time scale for the simulations presented here, the time for the projectile to move 2 nm is given at the top of Figure 3a,b. It is clear that the velocity of the particles in the >1 eV/nucleon region gives times to move 2 nm less than ∼100 fs. For the region below 1 eV/nucleon, however, the times are 200−400 fs. As was noted by Ryan et al. in simulations of C_n, $n = 6 \rightarrow 180$, clusters bombarding benzene, it is the time range for which the energy is no longer confined to the near surface region.[19,20] For bombardment by C_{180} at 5 keV (2 eV/nucleon), they observed that the energy deposited into the substrate was moving outward from the impact region before the projectile had deposited all of its energy. Thus, there was a reduced yield. This physics is key to the transition region observed in these simulations (Microscopic View).

The transition at 1 eV/nucleon is accompanied by an evolution of the amount of ejected fragments as shown in Figure 3d. For energies below 1 eV/nucleon, there are essentially no sputtered fragments, whereas above this value, the number of ejected fragments increases with incident energy. From an experimental viewpoint, there are two regions of interest. One region corresponds to a large signal of intact molecules. As shown in Figure 2b and ref 20, this condition can be met with higher energies. The other region corresponds to a low amount of ejected fragments. In order to highlight this region, in Figure 3c the ratio of the ejected mass of intact molecules divided by the total ejected mass is plotted vs the energy per nucleon. For the region above 1 eV/nucleon, half of the ejected mass is in intact molecules and half in fragments, independent of projectile and the energy. For

(58) Garrison, B. J.; Postawa, Z.; Ryan, K. E.; Vickerman, J. C.; Webb, R. P.; Winograd, N. *Anal. Chem.* **2009**, *81*, 2260.

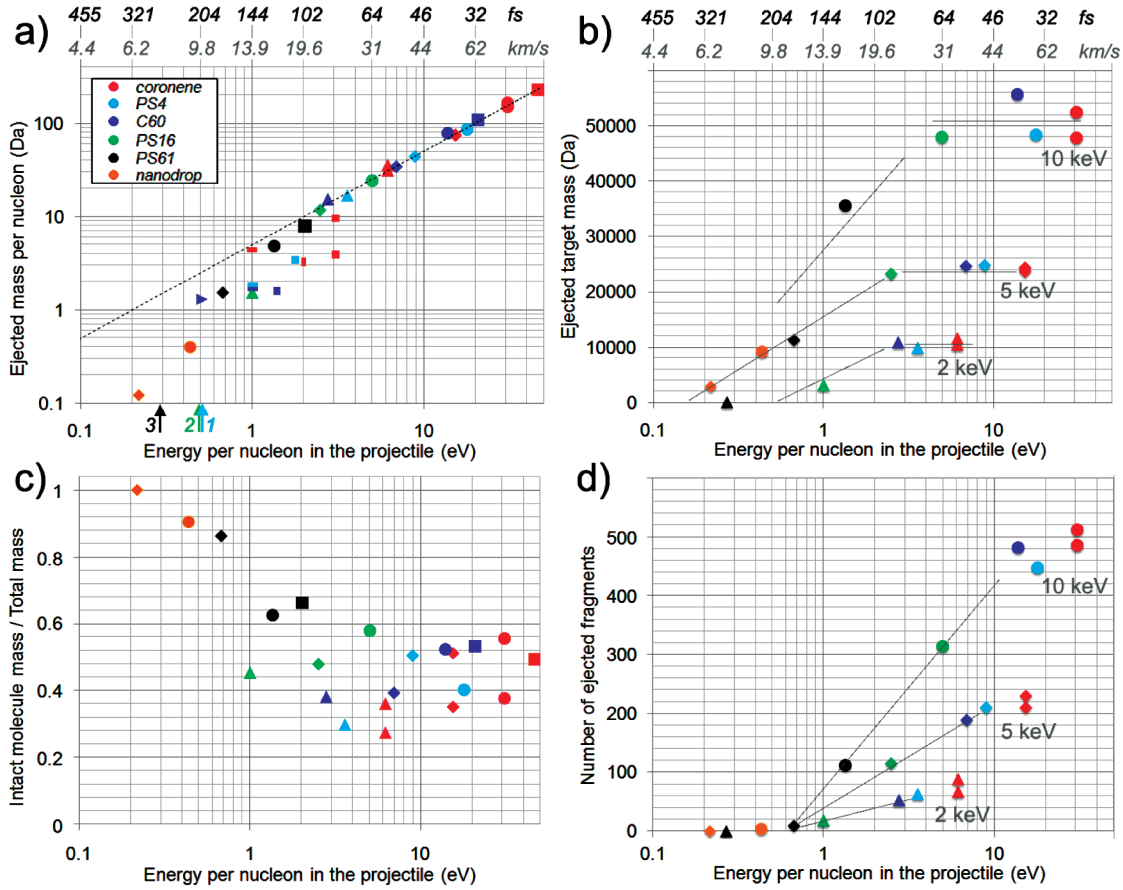

Figure 3. Regions of sputtering: (a) sputtered target mass per nucleon, (b) sputtered target mass, (c) fraction of the mass sputtered as intact molecules, and (d) number of sputtered fragments, as a function of the energy per nucleon in the projectile. Color coding determines the projectile (see legend in Figure 3a). Symbol shapes refer to the total energy of the projectiles: 1 keV, small squares; 2 keV, triangles; 5 keV, diamonds; 10 keV, circles; 15 keV, large squares. The upper scales indicate the projectile velocities in kilometer per second (in gray) and the corresponding time to travel 2 nm (in black). The light blue, green, and black arrows in Figure 3a indicate simulations for PS4 (280 eV), PS16 (1 keV), and PS61 (2 keV), respectively, in which the sputtered yield was zero.

the region below 1 eV/nucleon, the ratio is ~1 indicating that nearly all of the ejected material is intact molecules. It is important to add that small projectiles such as coronene, PS4, and C_{60} with 1 eV/nucleon are unable to sputter intact polyethylene oligomers.

There are experimental indications that low fragmentation can be attained with large noble gas clusters.[59−61] As a reference point, the mass of the nanodrop is about the same as an Ar_{560} cluster. For thick arginine, leucine, and triglycine films, fragmentation is strongly reduced when going from Ar_{300} to $Ar_{1500-2000}$ with the same acceleration energy (10 or 15 keV). For Ar_{1500} and Ar_{1750} clusters, it was shown that an increase of the projectile energy leads to increased fragmentation of arginine and triglycine.[59,60] Theoretically, a transition between soft desorption and fragmentation (Figure 3c,d) was also predicted for large Ar_n cluster bombardment of monolayers of benzene[62] and polystyrene[24] on silver. This transition arises at the energy of 5 eV/atom (or 0.12 eV/nucleon for Ar) vs ~1 eV/nucleon in our calculations. Saturation of the number of sputtered hydrocarbon fragments and intact molecules are also observed for the Ar bombarded monolayers, beyond 17 and 5 eV/atom, respectively, which is also significantly lower than our calculations (20 and 2 eV/nucleon, respectively). These differences indicate that the values are sensitive to the specific structures of the bombarded samples. In the monolayer systems, the observed saturation is probably governed by the limited number of molecules that are candidates for fragmentation and intact ejection. Consistently, the results obtained on monolayers also show that beyond 10 eV/atom, the projectile energy is increasingly dissipated in the heavy metal substrate, causing crater formation and emission of metal atoms.[24,62]

Microscopic View. In this section, we present the mechanistic aspects of the interaction between large molecular projectiles and organic materials, with a focus on the explanation of the transition observed in Figure 3a. The bombardment of polyethylene by a 10 keV nanodrop (0.43 eV/nucleon) is illustrated in Figure 4. In contrast with 10 keV C_{60} projectiles,[21] large molecular ensembles such as PS61 and the nanodrop, with energies around or below 1 eV/nucleon, do not fragment extensively upon impact. The situation at 0.75 ps clearly shows the pronounced compression of the projectile and target material upon impact (Figure 4b,c).

(59) Ninomiya, S.; Nakata, Y.; Ichiki, K.; Seki, T.; Aoki, T.; Matsuo, J. *Nucl. Instrum. Methods Phys. Res., Sect. B* **2007**, *256*, 493.
(60) Ninomiya, S.; Ichiki, K.; Nakata, Y.; Honda, Y.; Seki, T.; Aoki, T.; Matsuo, J. *Proceedings of the 8th Workshop on Cluster Ion Beam Technology*, Tokyo, Japan, November 8–9, 2007.
(61) Ichiki, K.; Ninomiya, S.; Nakata, Y.; Honda, Y.; Seki, T.; Aoki, T.; Matsuo, J. *Appl. Surf. Sci.* **2008**, *255*, 1148.
(62) Rzeznik, L.; Czerwinski, B.; Garrison, B. J.; Winograd, N.; Postawa, Z. *Appl. Surf. Sci.* **2008**, *255*, 841.

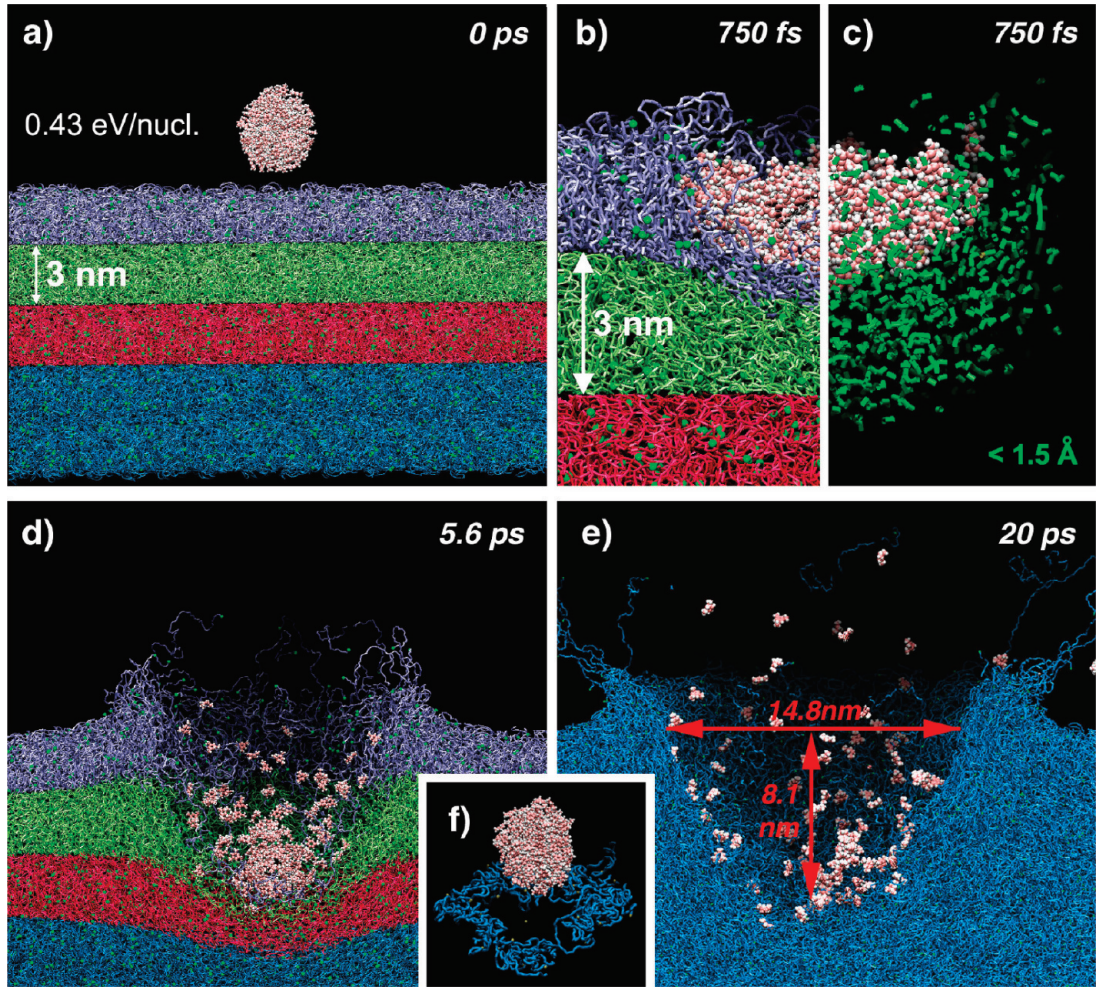

Figure 4. Time evolution of the interaction between a 10 keV organic nanodrop (0.43 eV/nucleon) and a polyethylene (1.4 kDa) molecular sample. (a, b, d, e) Side views at 0, 0.75, 5.6, and 20 ps. The iceblue, green, and red layers in part a are 3 nm thick at 0 ps. (c) Side view showing the C−C bonds in the target shortened by more than 0.03 Å (green). (e) Crater size at 20 ps. (f) Origin of the sputtered molecules (blue) at 0 ps (perspective view).

In Figure 4c, the region of the sample under compression is also detectable by the perturbation of the covalent bond lengths (shortened bonds in green). Side views of the dynamics at later times show that the projectile penetrates deeply into the sample surface and that the simultaneous outward motion of the sample molecules induces the formation of a wide crater surrounded by a rim (Figure 4d,e). The initial location of the sputtered molecules is an annular region directly surrounding the projectile (Figure 4f). The two types of molecules forming the nanodrop exhibit different behaviors. While the heavy polystyrene molecules agglomerate at the bottom of the crater, the lighter trimethylbenzenes tend to "evaporate" after 5 ps. This difference is probably due to the larger intermolecular attractive forces between the PS16 molecules and the surface and to their ability to deform together with the target molecules upon impact. In contrast, the smaller and stiffer trimethylbenzene molecules tend to stick less and to bounce back toward the vacuum.

Figure 4 indicates that a nanodrop with 0.43 eV/nucleon of energy is able to create a ~15 nm wide crater into polyethylene. For identical (total) impact energies, nanodrops create craters that are wider than those induced by fullerene impacts[21] but with less sputtering (Figures 2 and 3). Recently, the impact of large Ar_n clusters and C_{60} molecules on an organic crystal, solid benzene, have been theoretically compared.[15] In agreement with our results, Ar_n clusters were shown to generate larger craters but induce less sputtering than fullerenes. This observation appears therefore to be a general feature of the interaction of large clusters with organic surfaces. In contrast with our results, however, noble gas clusters dissociate and mostly evaporate after impact.

The domains of sputtering described in Figure 3 can be tentatively explained by measuring the dynamics of energy transfer in different parts of the sample, Figure 5. For that purpose, the top 3 nm of the sample surface was divided in a series of concentric rings around the impact point (Figure 5a). The first zone is a cylinder of 1.5 nm radius centered at the impact point. Other zones of interest are annular volumes of 1.5 nm thickness surrounding that central cylinder. The analysis of the sputtering process shows that, irrespective of the projectile nature, more than 90% of the bond scissions occur in the central zone.[35,58] On the other hand, intact molecular ejection occurs only from the outer areas (rings 1 and 2). Figure 5b−e shows the evolution of the average total energy per molecule ($C_{99}H_{200}$) as a function of time in each of these zones, for a selected subset of projectiles (C_{60}, PS16, PS61, nanodrop). This energy density is calculated as the sum of the energies of the atoms divided by the number of molecules present in the considered volume at each time.

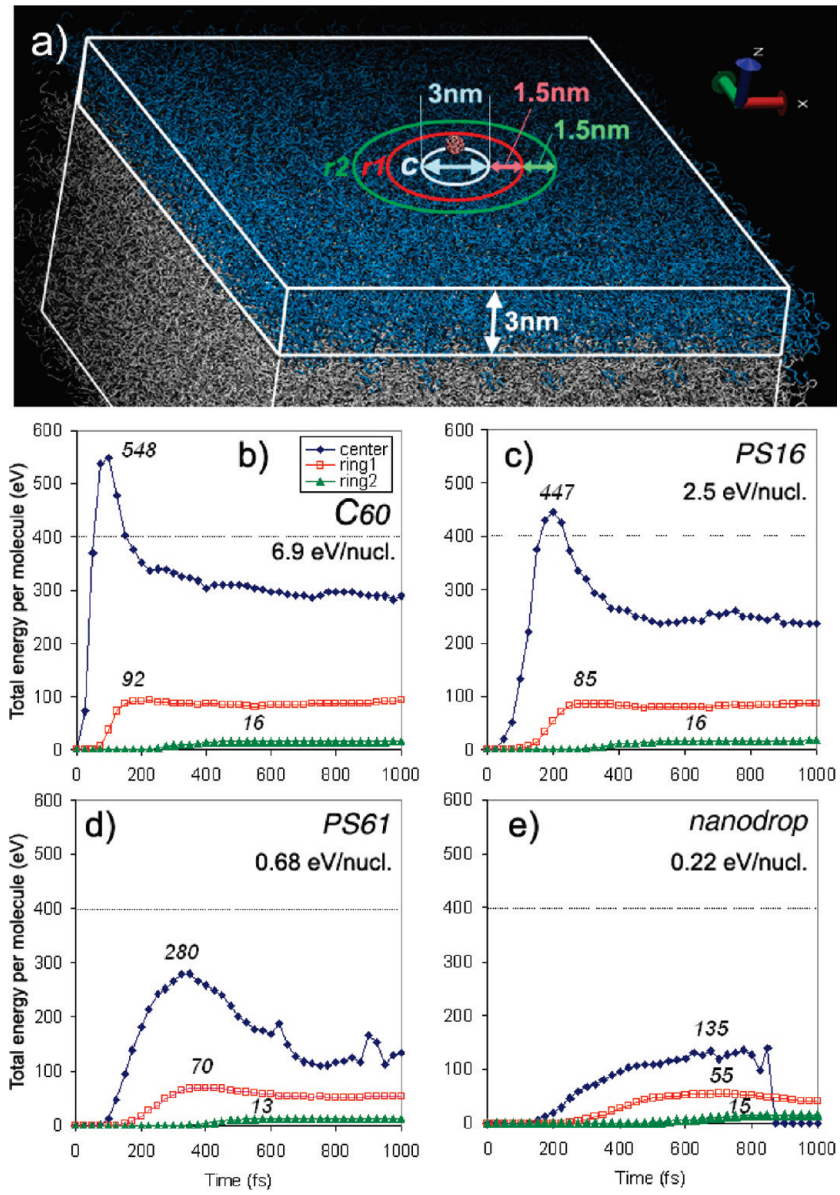

Figure 5. Dynamics of the energy transfer in the top 3 nm of the surface. (a) Definition of the central and peripheral zones with respect to the sample cell. (b−e) Time-evolution of the total energy per molecule deposited by the projectiles, C_{60} (b), PS16 (c), PS61 (d), and nanodrop (e) in the different zones: center, blue; ring 1, red; ring 2, green. The numbers in italic signify the maximum energy density (electronvolt/molecule) in each zone. The energy per nucleon in the projectile is also indicated.

First, the energy density attained in the central zone decreases strongly with decreasing projectile energy per nucleon. For projectiles with more than 1 eV/nucleon, (Figure 5b,c), the maximum energy density in that volume is higher than 400 eV, which corresponds to more than 4 eV per bond in our coarse-grained molecular model. Even though only a part of the energy goes directly into covalent bond excitation, these high energy densities explain why large numbers of bonds are broken in the early times of the interaction for relatively small projectiles. The time-evolutions of energy transfer are quite similar for projectiles with energy greater than 1 eV/nucleon. They show a pronounced peak in the central zone, followed by the transfer of energy in the peripheral rings (1 and 2). In terms of absolute energy values, the decrease after the maximum observed in the central volume corresponds almost quantitatively to the increase measured in ring 1 (taking into account the different volumes of the two regions). It confirms the sequential nature of the lateral energy transfer from one zone to the next. Above 1 eV/nucleon, all projectiles are depositing their energy in an optimal position in the substrate to contribute to the ejection process, which explains the independence of the yield on projectile type (Figure 3b).[20,22]

The situation is different for projectiles with less than 1 eV/nucleon (Figure 5d,e). (i) The energy transfer from the projectile is much slower, and the energy buildup in the different zones of the sample overlap in time. (ii) The maximum energy density in the considered surface volume (top 3 nm) is significantly lower. (iii) As a corollary, the energy simultaneously transferred in the depth of the sample is larger (not shown). In relation with previous studies and the MEDF model,[22] energy dissipation in the zone below the top ~3 nm appears to be wasted for sputtering. The energy draining out of the impact site before the projectile deposits all of its energy is reminiscent of the results for 5 keV C_{180} impinging on benzene.[20] The limited energy densities attained in the central volume also explain that fewer molecules become

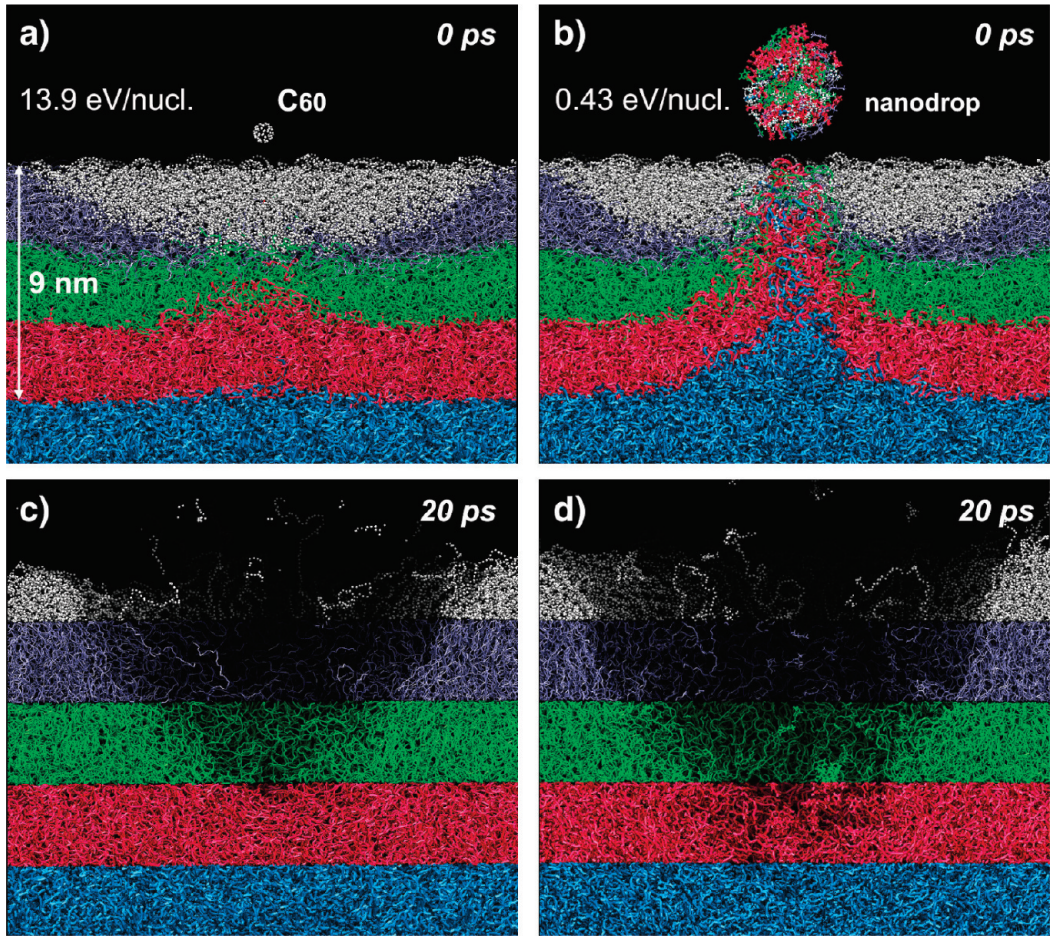

Figure 6. Material flow in the sample under 10 keV C_{60} (a,c) and nanodrop (b,d) impacts (13.9 and 0.43 eV/nucleon, respectively). The color coding is defined as a function of atom depth at 20 ps (c,d). The atoms are shown with the same colors at 0 ps (a,b). Atoms that are above the original surface plane at 20 ps are colored white.

fragmented. While the maximum energy density in the central zone is divided by 4 when going from C_{60} (6.9 eV/nucleon) to nanodrop projectiles (0.22 eV/nucleon), it is reduced by only 40% in ring 1 and it is almost unchanged in ring 2, where molecular ejection occurs. This observation explains why the indicators of fragmentation decrease faster than the number of molecules ejected intact with increasing projectile size, for a given total energy (Figures 2 and 3). Of note also is the fact that the average energy density in ring 1 is from 5 to 10 times larger than the binding energy per molecule (~9 eV), depending on the projectile, while it is always close to that energy in ring 2.

In other theoretical studies, it was shown that energetic atomic and small polyatomic projectiles (Au_3, small hydrocarbons) dissipate a larger fraction of their energy in the depth of the sample in comparison with larger aggregates (C_{60}), thereby limiting the sputtering yield.[15,19,20,22] For carbon-based projectiles under a certain energy per nucleon, i.e., beyond a certain molecular size at fixed total energy, a transition occurs toward another situation in which energy is transferred too deep in the sample to be effective and a concomitant reduction of the yield is observed again. The idea that the projectile energy must be dissipated in a well-defined volume, close to the sample surface, to induce maximum sputtering is therefore not challenged by the results involving large molecules.

The microscopic view of Figure 6 illustrates another implication of the two different domains of energy deposition, below and above 1 eV/nucleon, in terms of molecular motion and displacement in the target. The two projectiles chosen as examples are C_{60} with 13.9 eV/nucleon and the nanodrop with 0.43 eV/nucleon. To highlight molecular motion, the sample was color-coded by slices of 3 nm at the time of 20 ps so that the origin of the atoms in those final slices could be backtracked to the beginning of the trajectory by following the redistribution of the corresponding colors. White was used for atoms being above the original surface at 20 ps, i.e., atoms belonging to the crater rim or being ejected. The microscopic views at 20 ps (Figure 6c,d) simply confirm the larger volume of the crater induced by the nanodrop. In Figure 6a,b, one can see the site of origin of the molecular material that will be finally displaced in the colored slices of Figure 6c,d. The picture is quite different for C_{60} and the nanodrop. With C_{60}, except for the ejected and rim material displaced from the top layer, the stacking of the layers in the depth of the sample is only slightly modified by the impact, which indicates that the molecular motion giving rise to the crater is mainly lateral. In contrast, upon bombardment by the nanodrop, the overall molecular displacement shows a very pronounced vertical component. Some of the molecules belonging to the surface layer are pushed down to a depth of 10 nm (azure blue), at the bottom of the crater, as well as some constituents of the projectile. This pronounced vertical molecular motion is consistent with the transfer of a

large part of the energy in the depth of the sample, below the top 3 nm surface layer giving rise to molecular emission (the layer considered in Figure 5). Our results therefore predict that large molecular projectiles should induce more molecular mixing in organic samples than smaller clusters such as C_{60}.

The propagation of a pressure wave is observed in our simulations with all the considered projectiles. The wave velocity calculated from the MD results is 7.0 km/s for the impact of the slow nanodrop (0.43 eV nucleon), against 9.2 km/s for C_{60} (13.9 eV/nucleon). For comparison, the longitudinal speed of sound in polymers at room temperature, including polyethylene, is close to 2 km/s.[63] In the case of the nanodrop, the wave velocity is very close to the projectile velocity before impact (Table 1), but for C_{60} it is more than 5 times smaller. Together with the reduction of fragmentation and the analysis of the dynamics, this final observation confirms that by decreasing the energy per nucleon in the projectile, i.e., increasing the size of the molecular projectile for a given total energy, one moves from a situation of fast microscopic cluster impact, with velocities and time scales that are mismatched with the properties of the target in terms of molecular motion, to a situation of slower and macroscopic-like interaction, where the projectile remains essentially united and the target molecules collectively adapt and relocate as the projectile penetrates the solid.

Free Hydrogen in the Sample. An important issue for organic mass spectrometry, which constitutes the main application field of this study, concerns ionization. Experimentally, it is often observed that ionization proceeds via hydrogen or proton addition to form stable even electron ions. This mechanism is observed for both parent and fragment species. In this respect, it has been argued that cluster projectiles such as C_{60} might be able to enhance ionization in organic SIMS by increasing the number of free protons in the energized volume.[64,65] It is outside the scope of this study to introduce charge creation scenarios in the MD scheme. However, it might be informative to look at the fate of hydrogen atoms involved in the interaction. In particular we focus on two questions: (i) What are the effects of the projectile nature and energy on the number of free H atoms created in the crater? (ii) What fraction of these species arise from the decomposition of the projectile? To answer these questions, our coarse-grained representation of the sample is insufficient and running complete trajectories with a full atomistic model is not computationally tractable.[58] Nevertheless, the dynamics shows that ~90% of the bond-scissions occur in the first picosecond of the interaction and, within that time frame, the action is confined to a 5 nm diameter spherical volume at the surface.[35] Therefore, we decided to run a series of short-time, atomistic simulations with a smaller model sample made of short polyethylene-like chains (icosane, $C_{20}H_{42}$). Like our previous PE system, the structure of the icosane sample is amorphous (see computational details).

The number of free H species created upon impact of fullerene and hydrocarbon molecules with bulk icosane is reported in Figure 7. The first observation is that, in general, much larger

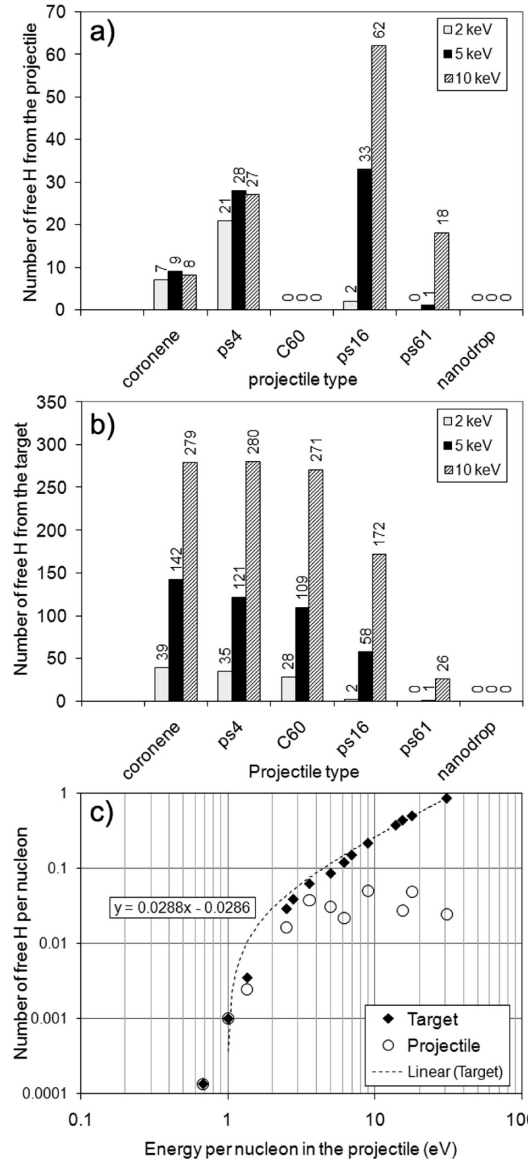

Figure 7. Numbers of H atoms liberated by the different molecular projectiles (with 2−10 keV of kinetic energy) in atomistic icosane: (a) from the projectile and (b) from the target. The corresponding numerical values are indicated above each bar. (c) Numbers of free H atoms per nucleon as a function of the energy per nucleon in the projectile (◆, H from the target; ○, H from the projectile).

numbers of free H atoms arise from the target (Figure 7b) than from the projectiles (Figure 7a). The maximum ratio of "projectile vs target" hydrogen creation is between 0.5 and 1 (0.6 for 2 keV PS4; 0.57 for 5 keV PS16; 0.69 for 10 keV PS61), but they correspond to situations where the total numbers are relatively low. The numbers of free H atoms created in the sample by small clusters (coronene → C_{60}) are consistent with recent simulations of C_{60} bombardment of octane and octatetraene substrates.[58] The PS61 and nanodrop create minimal free H atoms, in agreement with the description of the change in physics for the large projectile bombardment vs small projectile bombardment discussed in Sputtering Yields and Sputtering Regions. In Figure 7c, the results are presented with the same format as Figure 3a, that is, using scaled coordinates. The numbers of H atoms per nucleon created in the target fall on one single line. Therefore, in the considered limits of projectile type and energy,

(63) Hartmann, B.; Jarzynski, J. Report NOLTR 72-269, Naval Ordinance Laboratory: White Oak, Silver Spring, MD, 1972.
(64) Conlan, X. A.; Lockyer, N. P.; Vickerman, J. C. *Rapid Commun. Mass Spectrom.* **2006**, *20*, 1327.
(65) Winograd, N.; Postawa, Z.; Cheng, J.; Szakal, Ch.; Kozole, J.; Garrison, B. J. *Appl. Surf. Sci.* **2006**, *252*, 6836.

Figure 3c provides a simple chart to predict free hydrogen formation in an organic target. Despite the different formalism (full atomistic and coarse-grained models), the trends and quantitative values concerning fragmentation (Figure 3d) and H creation (Figure 7c) are in excellent agreement. Beyond the threshold at ~1 eV/nucleon (intercept of the linear regression at 0.99 eV), the number of free H atoms per nucleon in the target increases almost linearly, as did the yield (Figure 3a). The number of H atoms per nucleon liberated by the projectile and the target follow the same trend in the threshold region but the numbers corresponding to the projectile saturate beyond 2−3 eV/nucleon (5 keV PS16 or 2 keV PS4). This saturation can be explained by the limited number of H atoms in the projectile for large energies per nucleon (small projectiles). These results suggest that the hydrogen contained in hydrocarbon projectiles should not predominantly influence proton creation in the energized nanovolume for the range of energies usually sampled in the experiments.

Experimentally, higher yields of protonated molecules are measured with coronene than with C_{60} for samples including cyclosporin and cholesterol, but another sample, haloperidol, shows an opposite behavior.[66] In order to verify a possible effect of the hydrogen contained in the projectile on ionization, isotopically labeled projectiles should be used, in which all the H atoms should be replaced by deuterium. For instance, comparing the mass spectra obtained upon fully deuterated and regular coronene bombardment seems quite tractable. The presence (or the intensity variation) of molecular peaks shifted by one atomic mass unit would indicate ionization by a deuteron instead of a proton.

In the considered kinetic energy range, a detailed analysis shows that PS61 and the nanodrop are unable to induce diatomic collision energies that could lead to direct ionization (collision energies always below 10 eV). The situation is similar under EDI and MCI bombardment conditions, yet molecular secondary ions ($M^{+\bullet}$) are observed in these techniques for apolar polyaromatic hydrocarbon and fullerene targets.[67] One hypothesis that was proposed to explain ionization under these conditions involves electron−phonon coupling after the coherent phonon excitation induced by the subpicosecond compression of the target material.[37]

Better projectiles for molecular ionization might be clusters of "chemically active" molecules such as those used as a matrix in MALDI[68] or a spray solvent in DESI[69] and EDI.[70] For instance, acidic molecules could provide a low-energy channel for proton creation and transfer, probably more efficient than the physical effect investigated in these simulations. From the viewpoint of the dynamics, isobaric clusters of reactive molecules such as dihydroxybenzoic or trifluoroacetic acids should behave like the nanodrop.

CONCLUSION

Kiloelectronvolt organic molecules (0.3−23 kDa) bombarding polymeric surfaces create hemispherical nanocraters with a size that is primarily related to their total energy (~10 nm in diameter at 5 keV). Beyond a certain threshold depending on the projectile, they sputter a quantity of matter that is directly proportional to their energy. In the curve of the sputtered mass per nucleon vs energy per nucleon, a change of slope is observed around 1 eV. Beyond 1 eV/nucleon, the evolution is linear and identical for all the projectiles. Below that value, the yield induced by small clusters drops precipitously while the largest clusters display a specific, nonlinear behavior. This transition at 1 eV/nucleon is clearly connected with a change of fragmentation and free H creation in the target: at lower energies per nucleon and for large projectiles, fragmentation is minimal with a still significant yield of intact polyethylene oligomers (1.4 kDa). In contrast, small clusters such as coronene and C_{60} with 1 eV/nucleon of energy are unable to eject these large molecules. On the other hand, the impact of large molecular assemblies causes much more mixing in the sample than that of smaller clusters. In addition, they require higher kinetic energies to overcome the region of projectile deposition. Because of this combination of characteristics, their analytical capabilities for molecular depth profiling are questionable. Nonetheless, for molecular surface analysis, the region of soft-desorption sampled in these simulations appears to be of interest. Our results also indicate that, for saturated hydrocarbon samples, the number of free H atoms generated upon impact is not predominantly influenced by the H content of the projectile. Finally, with 0.2 eV/nucleon of energy, polystyrene oligomers embedded in a low-molecular weight matrix could be transferred intact onto polymeric surfaces (soft-landing).

ACKNOWLEDGMENT

This work and A.D. are supported by the Belgian Fonds National pour la Recherche Scientifique (FNRS). B.J.G. gratefully acknowledges the support of the National Science Foundation of America (NSF) through Grant CHE-0456514. B.J.G. would also like to acknowledge the support provided by the UK Engineering and Physical Sciences Research Council (EPSRC) under its Collaborating for Success through People initiative for a 3 month research visit with John Vickerman at the University of Manchester and Roger Webb at the University of Surrey, during which some of the ideas underlying this work were developed. K.H. is grateful to UCL for financial support through the FSR grant program. This work and K.H. were also supported by the French Community of Belgium via the Concerted Research Action programme (ARC NANHYMO: Convention 07/12-003). Computational resources were provided by the academic Services and Emerging technologies (ASET). The authors are also thankful to the ASET staff for assistance with the Lion-xe and Lion-xl clusters. The theoretical and computational biophysics group of the University of Illinois at Urbana−Champaign is acknowledged for the development and free access to the visualization software VMD.

Received for review April 7, 2009. Accepted June 23, 2009.

AC900746X

(66) Biddulph, G. X.; Piwowar, A. M.; Fletcher, J. S.; Lockyer, N. P.; Vickerman, J. C. *Anal. Chem.* **2007**, *79*, 7259.
(67) Mori, K.; Asakawa, D.; Sunner, J.; Hiraoka, K. *Rapid Commun. Mass Spectrom.* **2006**, *20*, 2596.
(68) Knochenmuss, R. *Analyst* **2006**, *131*, 966.
(69) Kauppila, T. J.; Wiseman, J. M.; Ketola, R. A.; Kotiaho, T.; Cooks, R. G.; Kostiainen, R. *Rapid Commun. Mass Spectrom.* **2006**, *20*, 387.
(70) Asakawa, D.; Fujimaki, S.; Hashimoto, Y.; Mori, K.; Hiraoka, K. *Rapid Commun. Mass Spectrom.* **2007**, *21*, 1579.